J. Shanghai Jiao Tong Univ. (Sci.), 2024
https://doi.org/10.1007/s12204-024-2720-5

# Magnetic Tracking System with Capability of Automatic Magnetic Moment Measurement

*TIAN Siyu*[1] (田思雨), *GAO Jinyang*[1,2*] (高晋阳), *HUANG Peng*[1] (黄　鹏), *MA Xinyu*[1] (马欣瑜), *MA Ziyu*[1] (马子毓)
(1. State Key Laboratory of Dynamic Measurement Technology, North University of China, Taiyuan 030051, China; 2. Key Laboratory of Micro/Nano Devices and Systems of Ministry of Education, North University of China, Taiyuan 030051, China)



**Abstract:** Magnetic tracking technologies have a promising application in detecting the real-time position and attitude of a capsule endoscope. However, most of them need to measure the magnetic moment of a permanent magnet (PM) embedded in the capsule accurately in advance, which can cause inconvenience to practical application. To solve this problem, this paper proposes a magnetic tracking system with the capability of measuring the magnetic moment of the PM automatically. The system is constructed based on a $4 \times 4$ magnetic sensor array, whose sensing data is analyzed to determine the magnetic moment by referring to a magnetic dipole model. With the determined magnetic moment, a method of fusing the linear calculation and Levenberg-Marquardt algorithms is proposed to determine the 3D position and 2D attitude of the PM. The experiments verified that the proposed system can achieve localization errors of 0.48 mm, 0.42 mm, and 0.83 mm and orientation errors of 0.66°, 0.64°, and 0.87° for a PM (⌀10 mm × 10 mm) at vertical heights of 5 cm, 10 cm, and 15 cm from the magnetic sensor array, respectively.

**Keywords:** permanent magnet, magnetic moment measurement, optimized Levenberg-Marquardt algorithm, MAG3110 magnetic sensor, tracking system
**CLC number:** R57, TM936.8　　**Document code:** A

## 0 Introduction

The tracking technology based on permanent magnet (PM) has been widely researched in recent years, such as medical fields (tracking of capsule endoscopes[1]) and industrial fields (tracking and navigation of automated guided vehicle[2], and position detection of motor[3-4]). Nowadays, there are three kinds of commonly-used tracking methods: the classical Levenberg-Marquardt (LM) algorithm, the optimized LM algorithm, and the neural network and deep learning method based on a large and high-resolution database.

The classical LM algorithm is a fast local search optimization algorithm. It is based on the principle of solving the inverse of a system of higher order nonlinear equations derived from the magnetic dipole model to determine the position and attitude of the PM. Schlageter et al.[5] implemented the PM tracking using the LM algorithm for the first time. However, the exact accuracy was not indicated. Subsequently, several studies have achieved tracking of a PM with the localization error typically around 5 mm. For example, Hu et al.[6] established a PM tracking system with a minimum localization error of 4.6 mm and provided a fast solution speed (0.137 s). Pham and Aziz[7] used the LM algorithm to track a capsule in an animal with a localization error of 5 mm. Song et al.[8] achieved real-time tracking wireless capsules with a localization error of up to 5.2 mm and an orientation error of 6.6° in dynamic scenarios.

However, the classical LM algorithm needs an initial solution close to the global optimal solution before the PM is positioned; otherwise, the results may converge to a local optimal solution. During the actual initial localization, the PM may appear at any position with any attitude[9]. To solve this problem, optimized LM algorithm, which is implemented by first solving the initial value problem and then substituting the

**Received:** 2023-05-23　**Accepted:** 2023-08-24
**Foundation item:** the National Natural Science Foundation of China (Nos. 52275038 and 61803347), the Shanxi Province Science Foundation for Excellent Youth (No. 202203021224007), the Key Research and Development Plan of Shanxi Province (No. 201903D321164), and the Opening Foundation of Shanxi Key Laboratory of Advanced Manufacturing Technology (No. XJZZ202101)
∗**E-mail:** gjy.1001@163.com

initial value into the classical LM algorithm to solve for the position and attitude of a PM, is proposed. Hu et al.[10] proposed a linear algorithm based on matrix and algebraic calculation to track a PM with average localization and orientation errors of 5.6 mm and 1.7° respectively. Then, they combined linear algorithm and LM algorithm to establish a system, whose tracking accuracy values were 1.8 mm and 1.6°, and the solution time was about 0.1 s[11]. Song et al.[12] fused the particle swarm optimization (PSO) algorithm and LM algorithm to track a PM with tracking accuracy values of 0.003 mm and 0.036°. However, the results showed that the execution time was up to 830 s, which could not meet the real-time requirement. Su et al.[13] established a magnetic tracking system based on LM algorithm and PSO algorithm. The most effective tracking distance is 36—96 mm, and the average tracking accuracy values are 0.70 mm and 1.22°. However, this effective tracking distance does not quite meet the human requirement yet. Su et al.[14] proposed intuitive method, a magnetic tracking approach based on LM algorithm, to solve the magnetic tracking problem based on graph optimization with average tracking accuracy values of 0.72 mm and 1.51°. However, the execution time of this algorithm is too long to meet the real-time requirement.

Meanwhile, the researchers proposed the use of neural networks and deep learning methods in magnetic tracking. Qin et al.[15] proposed a hybrid feed forward neural network and Levenberg-Marquardt (hFFNN-LM) algorithm to track a PM with tracking accuracy values of 0.70 mm and 0.90°, and the average single execution time was 1.07 ms. Sebkhi et al.[16] proposed a permanent magnet localization (PML) model that can achieve a localization error of 1.8 mm, but did not solve the attitude of a PM. Lv et al.[17] used the prior knowledge based back propagation neural network (PKBPNN) to track a PM in the far field (far source area), and the experiments showed that the average tracking accuracy values were 8.95 mm and 7.97° in a tracking range of 216—296 mm. However, high-precision tracking based on neural networks and deep learning requires a large and high-resolution database to support, and the database needs to be trained extensively before tracking.

In a word, it is clear that the optimized LM algorithm is the most cost-effective in terms of accuracy and real-time performance. However, this method requires pre-measurement of the magnetic moment. Currently, there are two methods to measure the magnetic moment of a PM. The first method is calculating its equivalent magnetic moment using a PM and a magnetometer[18]. The second method is implemented with a Helmholtz coil and a magnetometer[19], based on Biot-Savart Law and magnetic dipole model. However, these two methods are tedious and costly, which both require a high precision magnetometer to measure. And it is necessary to eliminate the influence of the earth's magnetic field and other constant stray magnetic fields on the magnetometer. Besides, keeping the PM as stationary relative to the magnetometer probe as possible is also indispensable.

To address the above limitation, this paper proposes a high-precision real-time magnetic tracking system that can measure the magnetic moment of PM automatically. The PM is placed at a specified position on the calibration board, and the magnetic moment is calculated based on the data sensed by the sensor and known parameters to achieve automatic measurement. Then the position and attitude of the PM are solved based on the magnetic moment and the optimized LM algorithm to realize the high precision real-time tracking of the PM.

This paper is organized as follows. Section 1 introduces the working flow of the tracking system and the method of magnetic moment measurement based on the magnetic dipole model. Section 2 introduces the optimized LM algorithm in detail. Section 3 introduces the experimental setup of the tracking system and analysis of experimental results. Finally, Sections 4 presents the conclusion.

## 1 Methodology

Figure 1 presents the working flow of the tracking system. First, the magnetic sensor array is configured by the single-chip microcomputer; the sensor array senses the magnetic induction intensity of the PM controlled by the robotic arm and outputs the sensing data to the multiplexer module. Second, the microcomputer controls the multiplexer module to select the 16 sensors in sequence and receives the sensing data from them; the sensing data is transmitted to MATLAB on the personal computer (PC). Finally, the optimized LM algorithm is used to solve for the position and attitude of the PM, and the tracking results are displayed on the computer interface in real time.

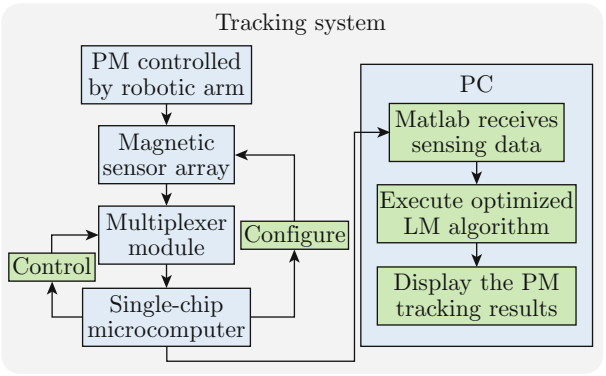


Fig. 1 Block diagram of the real-time and high-precision tracking system.

### 1.1 Magnetic Dipole Model

The magnetic dipole model is the basis of magnetic theory research, as shown in Fig. 2. Before studying the magnetic field distribution of a PM, it is necessary to know the spatial distribution of the magnetic field generated by a magnetic dipole.

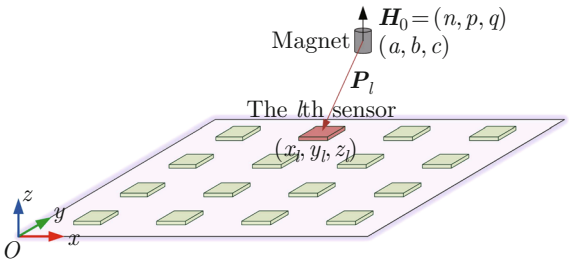


Fig. 2 Schematic of the magnetic dipole model.

The magnetic dipole is used as a simplified physical model for a cylindrical PM. The central point of the PM is $(a,b,c)$ and $\boldsymbol{H}_0=(n,p,q)$ represents the components of PM magnetization orientation on three coordinate axes. The spatial coordinates of the $l$th sensor are $(x_l,y_l,z_l)$, $1\leqslant l\leqslant 16$. The position vector of the PM with respect to the $l$th sensor is $\boldsymbol{P}_l=(x_l-a,y_l-b,z_l-c)$. According to the magnetic dipole model, the magnetic induction intensity at the $l$th sensor is

$$\begin{aligned}\boldsymbol{B}_l=&B_{lx}\boldsymbol{i}+B_{ly}\boldsymbol{j}+B_{lz}\boldsymbol{k}=\\&\frac{\mu_0\mu_{\rm r}m}{4\pi}\Big(\frac{3(\boldsymbol{H}_0\cdot\boldsymbol{P}_l)\boldsymbol{P}_l}{R_l^5}-\frac{\boldsymbol{H}_0}{R_l^3}\Big)=\\&B_{\rm T}\Big(\frac{3(\boldsymbol{H}_0\cdot\boldsymbol{P}_l)\boldsymbol{P}_l}{R_l^5}-\frac{\boldsymbol{H}_0}{R_l^3}\Big),\\&l=1,2,\cdots,16,\end{aligned}\tag{1}$$

where, $B_{lx}$, $B_{ly}$ and $B_{lz}$ are the 3-axis components of the magnetic induction intensity of the PM measured by the $l$th sensor; $\boldsymbol{i}$, $\boldsymbol{j}$ and $\boldsymbol{k}$ are the unit vectors of the $x$, $y$ and $z$ coordinate axes, respectively; $\mu_0$ is the vacuum magnetic permeability; $\mu_{\rm r}$ is the relative magnetic permeability; $m$ is the magnetic moment of the PM; $R_l$ is the modulus of $\boldsymbol{P}_l$, as

$$R_l=\sqrt{(x_l-a)^2+(y_l-b)^2+(z_l-c)^2}.\tag{2}$$

In this article, we propose a 5-D magnetic tracking system (3-D position and 2-D attitude). The cylindrical magnet can only provide 2-D rotation angles. Therefore, the following inherent constraint of the PM's attitude is added:

$$n^2+p^2+q^2=1.\tag{3}$$

Additionally, $B_{lx}$, $B_{ly}$ and $B_{lz}$ in Eq. (1) are expanded to obtain:

$$B_{lx}=\frac{\mu_0\mu_{\rm r}m}{4\pi}\times\Big\{\frac{3[n(x_l-a)+p(y_l-b)+q(z_l-c)](x_l-a)}{R_l^5}-\frac{n}{R_l^3}\Big\},\tag{4}$$

$$B_{ly}=\frac{\mu_0\mu_{\rm r}m}{4\pi}\times\Big\{\frac{3[n(x_l-a)+p(y_l-b)+q(z_l-c)](y_l-b)}{R_l^5}-\frac{p}{R_l^3}\Big\},\tag{5}$$

$$B_{lz}=\frac{\mu_0\mu_{\rm r}m}{4\pi}\times\Big\{\frac{3[n(x_l-a)+p(y_l-b)+q(z_l-c)](z_l-c)}{R_l^5}-\frac{q}{R_l^3}\Big\}.\tag{6}$$

We use the sensor to measure sensing data to calculate the magnetic moment $m$ of the PM. Based on the magnetic moment and the known parameters, the position $(a,b,c)$ and attitude $(n,p,q)$ of the PM can be solved by using the optimized LM algorithm, noted as $\boldsymbol{v}_0$.

### 1.2 Measure and Calculate Magnetic Moment

To solve the problem of inconvenience in the magnetic moment measurement of a PM, we use the magnetic sensor array to measure. The magnetic induction intensity of the PM used in the system is of Gauss magnitude within the tracking distance. However, the magnetic induction intensity of the earth's surface is about 0.5 Gauss. The magnetic field has an influence on the accuracy of magnetic tracking. Therefore, the interference to the sensors should be compensated before data collection. To effectively remove the interference during the sensor detection, bias measurement of the magnetic field can be performed and removed before tracking. The operation removes not only the earth's surface magnetic field, but also some other constant and stray magnetic fields. In this way, the subsequent sensing data is in better agreement with the magnetic induction intensity of the PM, which facilitates the precise tracking of the PM.

Figure 3 shows the flow chart of the magnetic moment calculation.

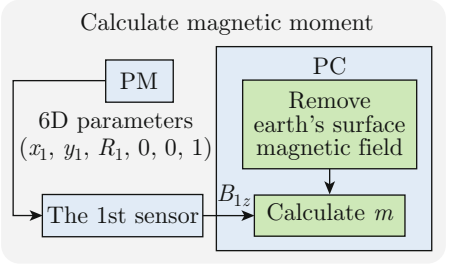


Fig. 3 Block diagram of magnetic moment calculation.

First, it is important to ensure that the sensing data is not disturbed by the earth's surface magnetic field

before calculating the magnetic moment. The process of compensating the interference is as follows: The PM used for the experiment is first placed away from the sensor array, which means that the sensors are not affected by the magnetic field of the PM. Each sensor of the array collects 20 sets of triaxial sensing data, and then calculates its mean separately as follows:

$$\left.\begin{aligned}\bar{B}_{lx}&=\sum_{t=1}^{20}B_{lx,t}\\ \bar{B}_{ly}&=\sum_{t=1}^{20}B_{ly,t}\\ \bar{B}_{lz}&=\sum_{t=1}^{20}B_{lz,t}\end{aligned}\right\},\quad l=1,2,\cdots,16, \tag{7}$$

where, $B_{lx,t}$, $B_{ly,t}$ and $B_{lz,t}$ represent the sensing data of the group $t$ collected by the $l$th sensor; $\bar{B}_{lx}$, $\bar{B}_{ly}$ and $\bar{B}_{lz}$ represent the mean of the $l$th sensor interference bias measurement.

Second, each sensor subtracts $(\bar{B}_{lx},\bar{B}_{ly},\bar{B}_{lz})$, the mean of the interference bias measurement, after collecting the sensing data. In this way the interference of the earth's surface magnetic field and other stray magnetic fields to the sensor is compensated. Then in order to simplify the calculation, only the magnetic induction intensity of the PM gathered on the single coordinate axis of the sensor is measured in actual magnetic moment measurement. Herein, we choose the $z$-axis to perform the calculation. The PM with fixed position and attitude $(x_1,y_1,R_1,0,0,1)$ is placed directly above the 1st sensor with fixed position $(x_1,y_1,0)$. After simplifying Eq. (6), $m$ can be expressed as follows:

$$m=\frac{2\pi B_{1z}R_1^3}{\mu_0\mu_{\rm r}}. \tag{8}$$

Finally, the data $(B_{1z})$ collected by the 1st sensor is transmitted to the PC through the multiplexer and the microcontroller. In addition, the magnetic moment $m$ is calculated according to Eq. (8).

It was experimentally verified that incorporating this method into the system, the entire process of magnetic moment measurement was less than 5 s. In addition, the magnetic moment of different sizes of PMs can be measured accurately. This method has significantly improved the accuracy and convenience of the magnetic moment measurement of capsules embedded with different sizes of PMs.

## 2 Optimized LM Algorithm

Figure 4 shows the flow chart of the optimized LM algorithm (linear calculation-LM): the sensors collect data and send it to the computer to execute the linear calculation once to estimate the position and attitude of the PM. The estimated result $\boldsymbol{v}_0(a_0,b_0,c_0,n_0,p_0,q_0)$ is used as the initial value for the LM algorithm. Then the LM algorithm is executed to obtain the exact position and attitude of the PM. The LM algorithm can be used separately for subsequent tracking, and the result of the previous solution is calculated as the initial value for the next solution until the end of the tracking task.

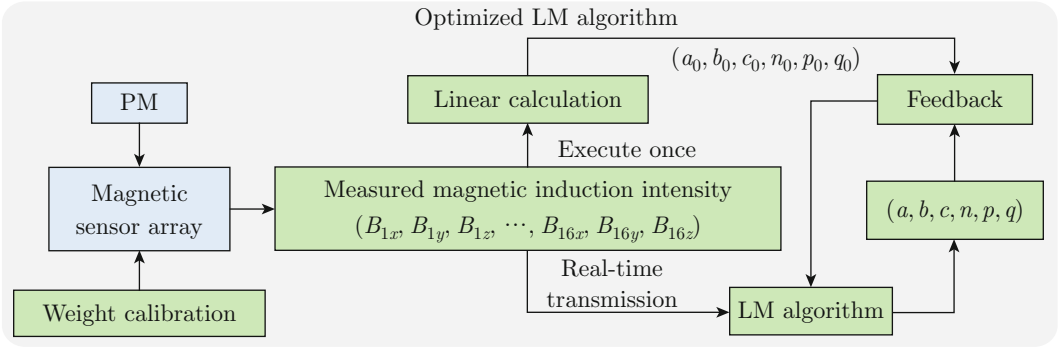


Fig. 4 Structure of the optimized LM algorithm.

The system achieves a high-precision tracking not only based on the accurate magnetic moment of PM and the optimized LM algorithm, but also on the weight calibration of the sensors to compensate for small quality differences between the different sensors. The weight factors are $\xi_{lx}$, $\xi_{ly}$ and $\xi_{lz}$, $1\leqslant l\leqslant 16$:

$$\xi_{lx}=\frac{B_{lx}}{B_{1x}},\quad \xi_{ly}=\frac{B_{ly}}{B_{1y}},\quad \xi_{lz}=\frac{B_{lz}}{B_{1z}}. \tag{9}$$

Then in the practical application of the algorithm, Eqs. (4)—(6) become the following:

$$B_{lx}=\frac{\xi_{lx}\mu_0\mu_{\rm r}m}{4\pi}\times \left\{\frac{3[n(x_l-a)+p(y_l-b)+q(z_l-c)](x_l-a)}{R_l^5}-\frac{n}{R_l^3}\right\}, \tag{10}$$

$$B_{ly}=\frac{\xi_{ly}\mu_0\mu_{\rm r}m}{4\pi}\times$$

$$\left\{\frac{3[n(x_l-a)+p(y_l-b)+q(z_l-c)](y_l-b)}{R_l^5}-\frac{p}{R_l^3}\right\}, \quad (11)$$

$$B_{lz}=\frac{\xi_{lz}\mu_0\mu_{\mathrm{r}}m}{4\pi}\times$$
$$\left\{\frac{3[n(x_l-a)+p(y_l-b)+q(z_l-c)](z_l-c)}{R_l^5}-\frac{q}{R_l^3}\right\}. \quad (12)$$

The detailed process of our proposed algorithm is as follows.

The first set of data measured by the magnetic sensor array is used to execute the linear calculation. The size of absolute of the data collected by the 16 sensors are compared, and the sensor with the largest sum of the 3-axis data's absolute is selected. Assign the position $(x_l, y_l)$ of the sensor to the initial parameter $(a_0, b_0)$. For example, if $\max\{|B_{1x}|+|B_{1y}|+|B_{1z}|, \cdots, |B_{16x}|+|B_{16y}|+|B_{16z}|\} = |B_{8x}|+|B_{8y}|+|B_{8z}|$, the position parameters are $(x_8, y_8, c_0)$. Then assign $c_0$ a value of 7.5 cm, 10 cm, or 12.5 cm according to the size of $|B_{8x}|+|B_{8y}|+|B_{8z}|$. The initial position parameters of the PM are obtained. Subsequent experiment verified that the linear calculation is easy to implement, and the approximate position parameters of the PM obtained from the linear calculation are used as the initial values of the LM algorithm, which can obtain the global optimal solution.

In order to fit the PM's position and attitude parameters more accurately, the following function based on Eq. (3) is constructed:

$$f = n^2 + p^2 + q^2 - 1. \quad (13)$$

The Jacobian function is utilized to fit the position and attitude parameters $\boldsymbol{v}(a, b, c, n, p, q)$. The partial derivatives of $a$, $b$, $c$, $n$, $p$ and $q$ in Eqs. (10)—(12) are solved using sensing data from 16 sensors, separately. Then partial derivatives of $a$, $b$, $c$, $n$, $p$ and $q$ in Eq. (13) are solved, separately. The Jacobian matrix with 49 rows and 6 columns is obtained as follows:

$$\boldsymbol{J}=\begin{bmatrix}
\frac{\partial B_{1x}}{\partial a} & \frac{\partial B_{1y}}{\partial a} & \frac{\partial B_{1z}}{\partial a} & \cdots & \frac{\partial B_{16x}}{\partial a} & \frac{\partial B_{16y}}{\partial a} & \frac{\partial B_{16z}}{\partial a} & 0\\
\frac{\partial B_{1x}}{\partial b} & \frac{\partial B_{1y}}{\partial b} & \frac{\partial B_{1z}}{\partial b} & \cdots & \frac{\partial B_{16x}}{\partial b} & \frac{\partial B_{16y}}{\partial b} & \frac{\partial B_{16z}}{\partial b} & 0\\
\frac{\partial B_{1x}}{\partial c} & \frac{\partial B_{1y}}{\partial c} & \frac{\partial B_{1z}}{\partial c} & \cdots & \frac{\partial B_{16x}}{\partial c} & \frac{\partial B_{16y}}{\partial c} & \frac{\partial B_{16z}}{\partial c} & 0\\
\frac{\partial B_{1x}}{\partial n} & \frac{\partial B_{1y}}{\partial n} & \frac{\partial B_{1z}}{\partial n} & \cdots & \frac{\partial B_{16x}}{\partial n} & \frac{\partial B_{16y}}{\partial n} & \frac{\partial B_{16z}}{\partial n} & \frac{\partial f}{\partial n}\\
\frac{\partial B_{1x}}{\partial p} & \frac{\partial B_{1y}}{\partial p} & \frac{\partial B_{1z}}{\partial p} & \cdots & \frac{\partial B_{16x}}{\partial p} & \frac{\partial B_{16y}}{\partial p} & \frac{\partial B_{16z}}{\partial p} & \frac{\partial f}{\partial p}\\
\frac{\partial B_{1x}}{\partial q} & \frac{\partial B_{1y}}{\partial q} & \frac{\partial B_{1z}}{\partial q} & \cdots & \frac{\partial B_{16x}}{\partial q} & \frac{\partial B_{16y}}{\partial q} & \frac{\partial B_{16z}}{\partial q} & \frac{\partial f}{\partial q}
\end{bmatrix}^{\mathrm{T}}. \quad (14)$$

The specific Jacobian matrix is obtained by substituting the known parameters $(x_l, y_l, z_l)$, $(B_{lx}, B_{ly}, B_{lz})$, $\xi_{lx}$, $\xi_{ly}$, $\xi_{lz}$, $m$, $\mu_0$, $\mu_{\mathrm{r}}$ and $\boldsymbol{v}_0$ into Eq. (14). In order to obtain the accurate position and attitude parameters of PM, the errors between the calculated data $(B_{lx}, B_{ly}, B_{lz}, f)$ based on the fitted parameters $(\boldsymbol{v}_0)$ and the actual data $(B_{lx}^*, B_{ly}^*, B_{lz}^*, f^*)$ measured by the sensors need to be minimized. We define the objective error function as follows:

$$E=\sum_{l=1}^{16}(B_{lx}^*-B_{lx})^2+\sum_{l=1}^{16}(B_{ly}^*-B_{ly})^2 + \sum_{l=1}^{16}(B_{lz}^*-B_{lz})^2+f^*-f, \quad (15)$$

where, $B_{lx}$, $B_{ly}$ and $B_{lz}$ are calculated by Eqs. (10)—(12), $B_{lx}^*$, $B_{ly}^*$ and $B_{lz}^*$ are the measured sensing data by the $l$th 3-axis magnetic sensor, $1 \leqslant l \leqslant 16$, $f^* \equiv 0$ is known from the inherent constraint Eq. (3), and $f$ is calculated from the initial parameters $(n_0, p_0, q_0)$ according to Eq. (13). The known parameters are substituted into the Eq. (15) to obtain the error before the calculation of the first iteration. The differences between $B_{lx}^*$, $B_{ly}^*$, $B_{lz}^*$, $f^*$ and $B_{lx}$, $B_{ly}$, $B_{lz}$, $f$ $(1 \leqslant l \leqslant 16)$ are as follows:

$$\left.\begin{aligned}
d_1 &= B_{1x}^* - B_{1x}\\
d_2 &= B_{1y}^* - B_{1y}\\
d_3 &= B_{1z}^* - B_{1z}\\
&\vdots\\
d_{46} &= B_{16x}^* - B_{16x}\\
d_{47} &= B_{16y}^* - B_{16y}\\
d_{48} &= B_{16z}^* - B_{16z}\\
d_{49} &= f^* - f
\end{aligned}\right\}. \quad (16)$$

The error matrix $\boldsymbol{E}$ is shown in

$$\boldsymbol{E}=[d_1\ d_2\ d_3\ \cdots\ d_{46}\ d_{47}\ d_{48}\ d_{49}]. \quad (17)$$

The incremental normal matrix is constructed as

$$\boldsymbol{h} = \boldsymbol{J}^{\mathrm{T}}\boldsymbol{E}^{\mathrm{T}}/(\boldsymbol{J}\boldsymbol{J}^{\mathrm{T}} + \lambda\boldsymbol{I}), \tag{18}$$

where, $\boldsymbol{J}^{\mathrm{T}}$ and $\boldsymbol{E}^{\mathrm{T}}$ are the transpose matrices of $\boldsymbol{J}$ and $\boldsymbol{E}$, respectively; $\lambda$ is the damping factor to regulate the speed of iteration; $\boldsymbol{I}$ is the 6th order unit matrix. The specific incremental matrix is obtained by substituting known parameters into Eq. (18):

$$\boldsymbol{h} = [\Delta a\ \Delta b\ \Delta c\ \Delta n\ \Delta p\ \Delta q]. \tag{19}$$

The six increments of Eq. (19) are added to the initial parameters $(a_0, b_0, c_0, m_0, n_0, p_0)$ in turn, and then the fitted position and attitude parameters are obtained after the first iteration:

$$\begin{aligned}\boldsymbol{v}_1 = &(a_0 + \Delta a, b_0 + \Delta b, c_0 + \Delta c,\\ &n_0 + \Delta n, p_0 + \Delta p, q_0 + \Delta q) =\\ &(a_1, b_1, c_1, n_1, p_1, q_1).\end{aligned} \tag{20}$$

The newly calculated data $\boldsymbol{B}_l(B_{lx}, B_{ly}, B_{lz})$ and $f$ are obtained by substituting $\boldsymbol{v}_1$ into Eqs. (10)—(13). Then the newly calculated data $\boldsymbol{B}_l(B_{lx}, B_{ly}, B_{lz})$, $f$ and the measured data $\boldsymbol{B}_l^*(B_{lx}^*, B_{ly}^*, B_{lz}^*)$, $f^*$ are substituted into Eq. (15) to calculate the fitted error $(E')$.

The errors ($E$ and $E'$) before and after the fitting of the position and attitude parameters of PM are compared. If the new error after fitting $(E')$ is smaller than the error before fitting $(E)$, the damping factor $(\lambda)$ is adjusted to 1/10 of the original one. The next iteration is executed using the newly fitted position and attitude parameters $(\boldsymbol{v}_1)$ of the PM. The solving is terminated when the iterative operation reaches the maximum number of iterations. The final fitted position and attitude parameters $(\boldsymbol{v})$ of the PM are obtained. Conversely, the damping factor $(\lambda)$ is adjusted to 10 times the original one and the iterative operation is continued to the end to obtain the optimal parameters $\boldsymbol{v}(a, b, c, n, p, q)$.

## 3 Experimental Verification

### 3.1 Magnetic Tracking System

The magnetic tracking system, which consists of a PM, a magnetic sensor array (a multiplexer module and 16 sensors), a single-chip microcomputer, a calibration board and a six-axis robotic arm, is shown in Fig. 5. Three types of PMs used in the experiments are all commonly-used sizes (with sizes of ∅8 mm × 8 mm, ∅10 mm × 10 mm and ∅12 mm × 6 mm) that are suitable for embedding in capsules. The PM is positioned by a robotic arm in the 25 cm × 25 cm × 15 cm workspace, which is above the $4 \times 4$ magnetic sensor array with each sensor spacing 7 cm. The sensor array is constructed of 16 sensors fixed on an acrylic board and a multiplexer module. Dimensions of the calibration board and the sensor array board are the same, and the adjustable support legs between them are perpendicular to the two boards. The single-chip microcomputer (STM32F103) obtains the real-time sensing data from the sensors via the multiplexer module, which is constructed of CD4067 analog multiplexer/demultiplexer controlled by the microcomputer. The sensing data transmission between the microcomputer and sensors is based on the inter integrated circuit (IIC) bus. Then the data is transmitted to the computer through the serial port. The computer is used for executing optimized LM algorithm and displaying the PM's position and attitude in real time. Six-axis robotic arm (DOBOT CR5) is used for controlling non-directional movement of the PM with tracking accuracy values of ±0.03 mm and ±0.02°, and verifying the localization and orientation accuracy of the system.

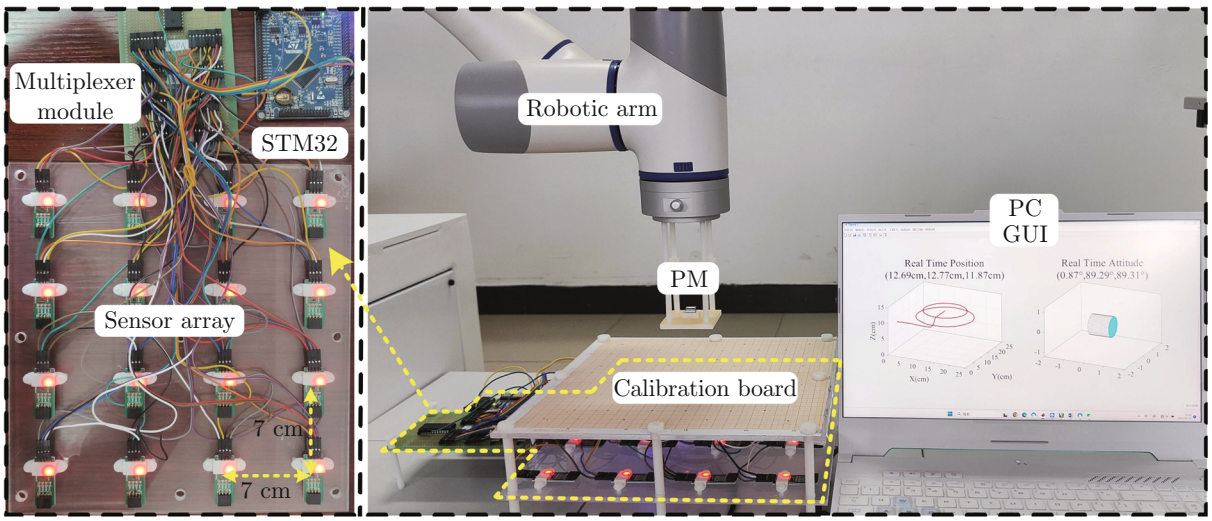


Fig. 5 Experimental setup of the proposed tracking system.

In order to select suitable sensor, a finite-element software (COMSOL) is used to establish a model to simulate the spatial distribution of the magnetic field of two of the PMs (the smallest: ∅8 mm × 8 mm and largest size: ∅10 mm × 10 mm) used in the experiments, separately.

Figures 6(a) and 6(d) are the dimensional drawings of the two PMs. Figures 6(b) and 6(c) are spatial distribution diagram of two PMs's magnetic fields that simulated by COMSOL, respectively. The vertical detection distance of the tracking system is 5—15 cm. The simulation results show that the maximum magnetic induction intensity that the sensor can collect during the tracking is about 604 μT and the minimum is about 1 μT.

Table 1 shows the important parameters of three

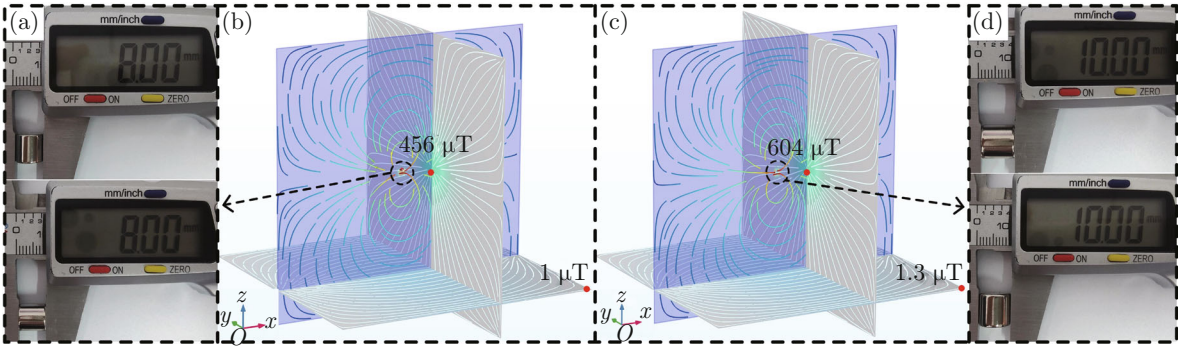


Fig. 6 Simulation results. (a) Size of ∅8 mm × 8 mm magnet; (b) Simulation result of ∅8 mm × 8 mm magnet; (c) Simulation result of ∅10 mm × 10 mm magnet; (d) Size of ∅10 mm × 10 mm magnet.

**Table 1 Comparison of sensor performance**

| Sensor type | Magnetic induction intensity/μT | | | Sampling rate/Hz |
|---|---|---|---|---|
| | Full scale range | Sensitivity | Noise | |
| HMC5883L[8] | ±800 | 1 | 0.5 (min) | 75 |
| MLX90393[20] | ±5 000 | 0.6 | 0.2 (min) | 90 |
| MAG3110 | ±1 000 | 0.10 | 0.05 (RMS) | 80 |

kinds of sensors. According to these parameters, the maximum magnetic induction intensity (604 μT) collected by the sensor in the system is within the maximum range (1 000 μT). The minimum magnetic induction intensity (1 μT) is much greater than the sensitivity (0.10 μT) and noise value (0.05 μT) of the sensor. Because the basis of accurate tracking of the system is that the sensors can collect data that have effective changes when the PM moves a small distance. In addition, the data transmission rate of the sensor meets the real-time requirements of the tracking system. After comparing, we chose MAG3110 3-axis digital magnetometer with high sensitivity and low noise.

The specific design of the sensor array is as follows: the power, ground, and clock of the 16 sensors share a common pathway, separately. In addition, they are connected to the three pins (VCC, GND, SCL) corresponding to the multiplexer module. The pins of the 16 sensors for transmitting data are connected to each of the 16 conduction channels ($I_{1-16}/O_{1-16}$) of the multiplexer module. The microcontroller connects and controls the inputs ($A_0$—$A_3$) of the multiplexer module to select its 16 conduction channels and then its serial data (SDA) outputs the sensing data of 16 sensors in sequence. The microcontroller receives the data and transfers it to the computer for processing. This design is simple and stable for data transmission and easy to apply.

### 3.2 Linear Calculation Result

According to Ref. [11], the localization and orientation errors can converge to zero when the localization error of the LM algorithm's initial solution is within 20 cm. We selected 36 sampling points to place the PM. Then the computer executes linear calculation to estimate the position of the PM. To evaluate the performance of the tracking accuracy, we define two parameters, localization error ($E_l$) and orientation error ($E_o$) as follows:

$$\left.\begin{aligned} &e_a = a_c - a_t, \quad e_b = b_c - b_t, \quad e_c = c_c - c_t \\ &E_l = \sqrt{(e_a)^2 + (e_b)^2 + (e_c)^2} \end{aligned}\right\}, \tag{21}$$

$$\left.\begin{aligned} &e_n = \arccos n_c - \arccos n_t \\ &e_p = \arccos p_c - \arccos p_t \\ &e_q = \arccos q_c - \arccos q_t \\ &E_o = \sqrt{(e_n)^2 + (e_p)^2 + (e_q)^2} \end{aligned}\right\}, \tag{22}$$

where, $(a_c, b_c, c_c, n_c, p_c, q_c)$ represents the calculated position and attitude parameters of the PM; ($a_t$, $b_t$, $c_t$, $n_t$, $p_t$, $q_t$) represents the true parameters; $e_a$, $e_b$, $e_c$ and $e_n$, $e_p$, $e_q$ represent the localization errors and orientation errors, respectively. To enhance the readers' understanding of the paper, the errors of $n$, $p$, $q$ are

converted to the angular errors of the attitude of the PM.

Table 2 shows that the total localization absolute error is 3.05 cm, well below 20 cm. The executing result of linear calculation is used as the initial solution of the LM algorithm, so linear calculation is reliable.

**Table 2 Localization absolute error of linear calculation**

| Samples | Localization absolute error/cm | | | Total $E_1$/cm |
|---|---|---|---|---|
| | $\|e_a\|$ | $\|e_b\|$ | $\|e_c\|$ | |
| 36 | 1.71 | 1.57 | 1.98 | 3.05 |

### 3.3 Specific Trajectory Experiments

Figures 7(a)—7(c) respectively show the results from the same experiment on three trajectories with the three PMs moving at a speed of 22.3 mm/s and show the truth trajectory (blue) and the estimated trajectory(red) of the three PMs. Figures 7(d)—7(f) evaluate the localization and orientation accuracy of the three sizes of PMs during the movement in Figs. 7(a)—7(c), respectively. The red dashed lines show the average localization and orientation absolute errors. The errors for the experiments with three PMs of dimensions ∅8 mm × 8 mm, ∅10 mm × 10 mm, and ∅12 mm × 6 mm are 1.41 mm and 1.68°, 1.21 mm and 1.27°, and 1.31 mm and 1.55°, respectively. Experiments with the three different sizes of PMs were used to verify the proposed method for measuring magnetic moment. It was demonstrated that the magnetic moment of different sizes of PMs can be measured with high accuracy and applied in the tracking system to solve the position and attitude of the PM. The data shows the PM with a size of ∅10 mm × 10 mm achieves the highest accuracy.

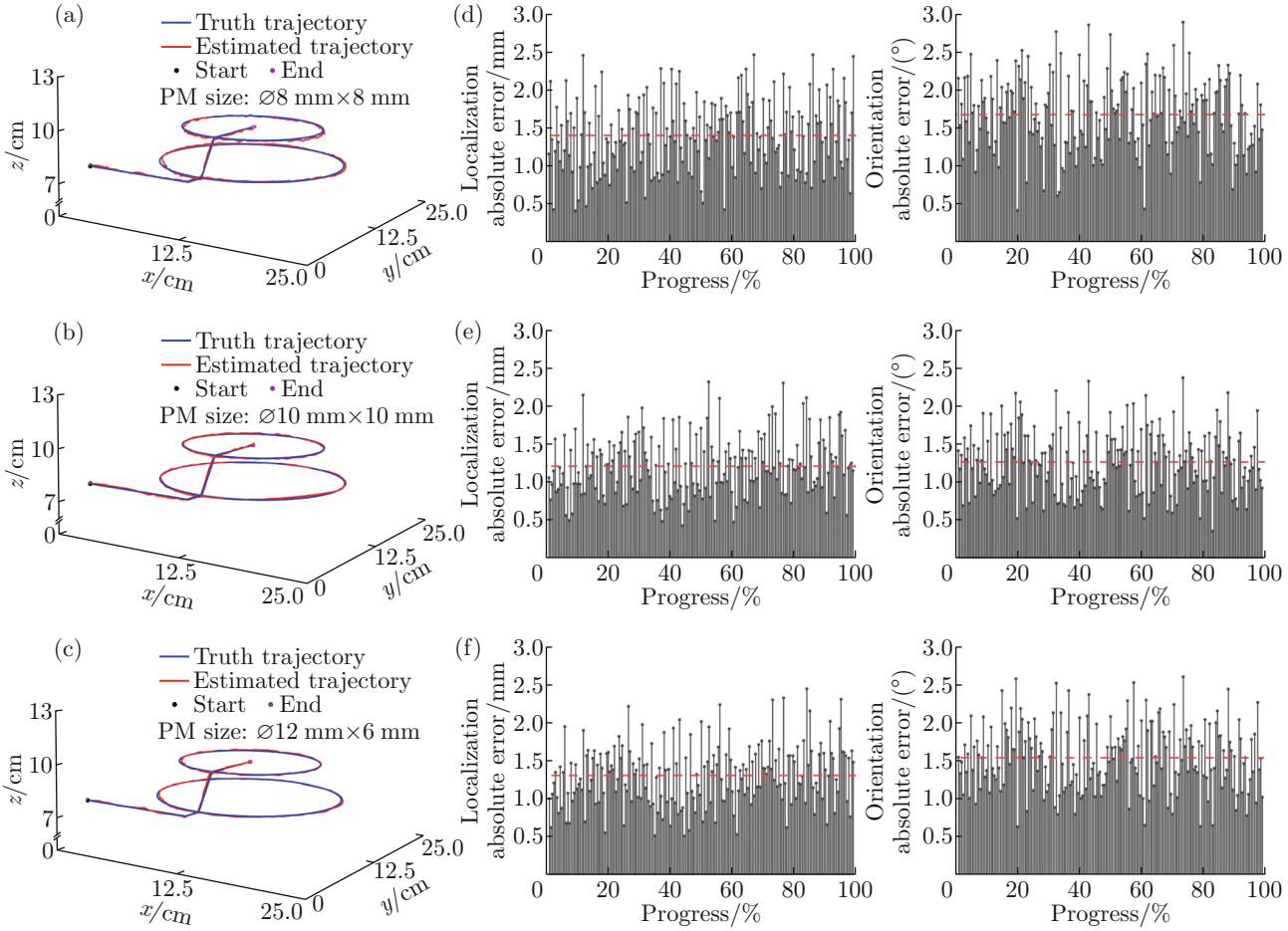


Fig. 7 Tracking trajectory and tracking accuracy of the three PMs. (a), (b), (c) Tracking trajectories of PMs; (d) Tracking accuracy of the trajectory in Fig. 7(a); (e) Tracking accuracy of the trajectory in Fig. 7(b); (f) Tracking accuracy of the trajectory in Fig. 7(c).

Figure 8 shows the experimental process of the system tracking the PM (∅10 mm × 10 mm) in real time and show the position and attitude of the actual PM (controlled by the robotic arm) and the PM fitted by the system (shown by GUI). Figures 8(a)—8(d) are four figures of the trajectory and attitude of the PM

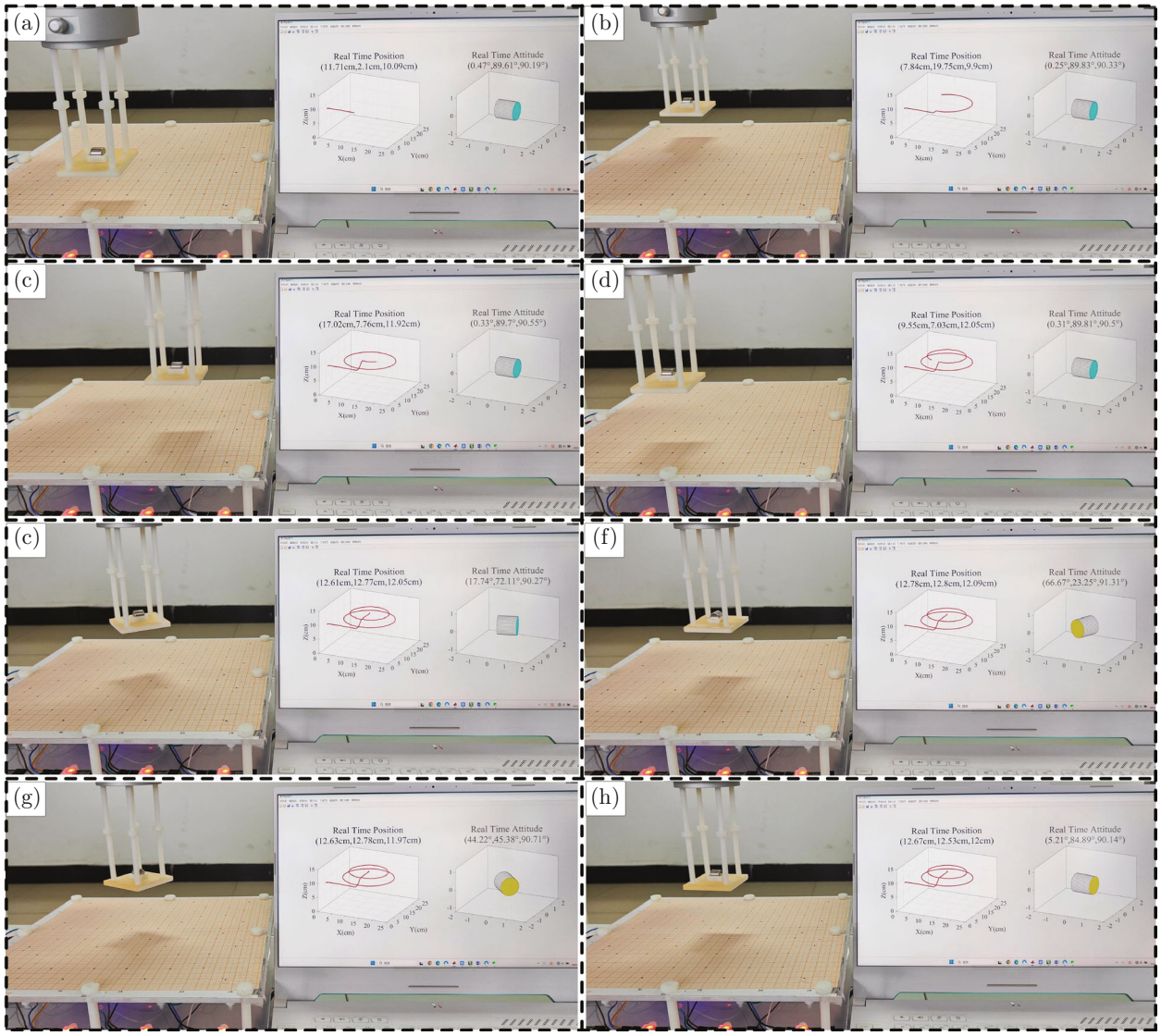


Fig. 8 Experimental process of system real-time tracking the PM. (a)—(d) Changing the position of the PM's motion; (e)—(h) Changing the attitude of the PM's motion.

with fixed attitude moving in the workspace. And Figs. 8(e)—8(h) are four figures of the trajectory and attitude of the PM with fixed position changing its attitude in the workspace. In order to evaluate the localization and orientation accuracy specifically, we conducted quantitative experiments.

### 3.4 Quantitative Experiments

In quantitative experiments, the PM was positioned at 8 × 8 evenly spaced positions spanning 25 cm × 25 cm on three horizontal planes with an increasing height of 5 cm to 15 cm, resulting in a total of 192 test poses. Figures 9(a)—9(c) show the truth positions of the PM (blue) and the estimated positions (red) corresponding to the three horizontal planes at different heights as shown in Fig. 9(d), respectively. Specifically, the PM was controlled to move along the trajectory as shown in Figs. 9(a)—9(c) (blue lines) to reach all the test positions. The estimated positions by our method are illustrated in red.

Tables 3 and 4 show the localization and orientation accuracy of the tracking system, respectively. The accuracy represented by the mean and standard deviations of the localization and orientation errors of each axis is based on the quantitative experiment, respectively. The average localization errors across the 192 test poses in the 25 cm × 25 cm × 15 cm workspace are 0.33 mm, 0.30 mm, and 0.36 mm in $x$, $y$, and $z$ axes, respectively, and the average orientation errors are 0.43°, 0.39°, and 0.43° in $x$, $y$, and $z$ axes, respectively. As shown in Tables 3 and 4, compared with 5 cm and 15 cm horizontal planes, the PM has the highest tracking accuracy on the 10 cm horizontal plane. The tracking system maintains high tracking accuracy even on the 15 cm horizontal plane.

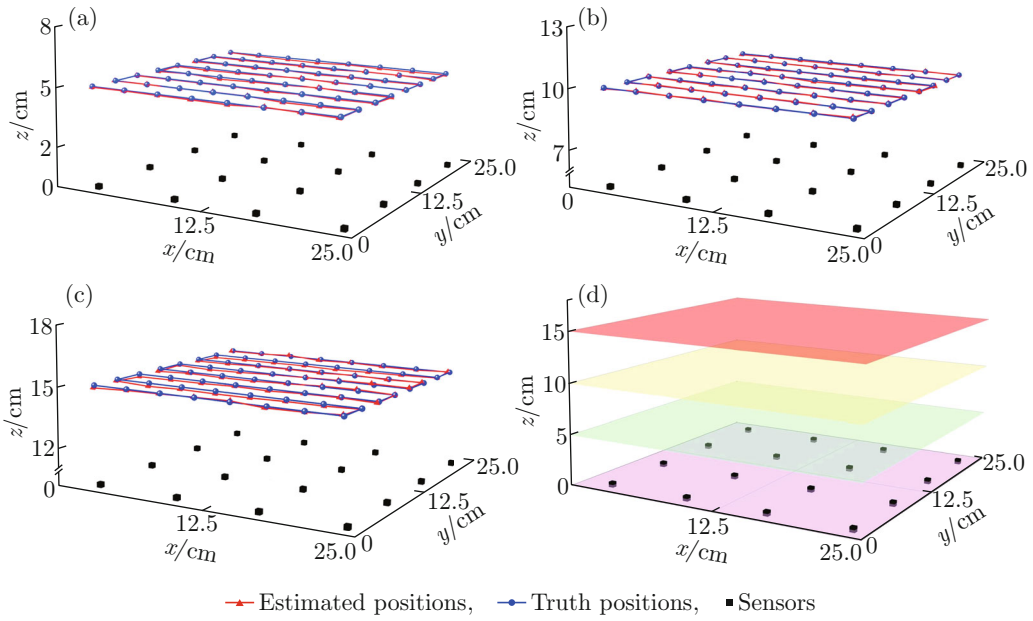


Fig. 9 Quantitative tracking experiments. (a) 5 cm height test experiment; (b) 10 cm height test experiment; (c) 15 cm height test experiment; (d) Three test heights.

**Table 3 Localization accuracy (mean error ± standard deviation) for quantitative experiments at 192 poses with three heights in the 25 cm × 25 cm × 15 cm workspace**

| Height/mm | Number of poses | Localization error/mm | | | Total $E_l$/mm |
|---|---|---|---|---|---|
| | | $e_a$ | $e_b$ | $e_c$ | |
| 50 | 64 | $0.26 \pm 0.53$ | $0.22 \pm 0.56$ | $0.34 \pm 0.65$ | $0.48 \pm 0.58$ |
| 100 | 64 | $0.23 \pm 0.49$ | $0.26 \pm 0.52$ | $0.23 \pm 0.56$ | $0.42 \pm 0.52$ |
| 150 | 64 | $0.49 \pm 0.63$ | $0.43 \pm 0.73$ | $0.51 \pm 0.59$ | $0.83 \pm 0.65$ |
| Total | 192 | $0.33 \pm 0.55$ | $0.30 \pm 0.60$ | $0.36 \pm 0.60$ | $0.58 \pm 0.58$ |

**Table 4 Orientation accuracy (mean error ± standard deviation) for quantitative experiments at 192 poses with three heights in the 25 cm × 25 cm × 15 cm workspace**

| Height/mm | Number of poses | Orientation error/(°) | | | Total $E_o$/(°) |
|---|---|---|---|---|---|
| | | $e_n$ | $e_p$ | $e_q$ | |
| 50 | 64 | $0.41 \pm 0.87$ | $0.37 \pm 0.76$ | $0.36 \pm 0.70$ | $0.66 \pm 0.78$ |
| 100 | 64 | $0.38 \pm 0.83$ | $0.34 \pm 0.70$ | $0.38 \pm 0.66$ | $0.64 \pm 0.73$ |
| 150 | 64 | $0.51 \pm 1.07$ | $0.45 \pm 0.97$ | $0.54 \pm 1.06$ | $0.87 \pm 1.03$ |
| Total | 192 | $0.43 \pm 0.92$ | $0.39 \pm 0.81$ | $0.43 \pm 0.81$ | $0.72 \pm 0.85$ |

At the same time, temperature has an effect on both the magnetic moment of the PM and the resistivity of the sensor. The magnetic induction intensity measured by the magnetic sensor is different for the same PM placed in the same position at different temperatures. When the surrounding temperature of the system in working changes, the error of the system in tracking the PM would become larger. So we have performed temperature compensation, which is re-measuring the magnetic moment before each experiment. It can be understood as ensuring the same ratio between the sensing data and the real magnetic induction intensity data by changing the magnetic moment. We conducted three experiments at different temperatures (20 °C, 25 °C, and 30 °C). Table 5 shows that the measured magnetic moment values at three different common room temperatures are indeed different, but the changes in the localization errors and orientation errors of the system are almost negligible.

The factors that affect the real-time performance of

**Table 5 Tracking accuracy of the system at different temperatures**

| Temperature/ °C | Height/ cm | Magnetic moment/ $(A \cdot m^2)$ | Total $E_l$/mm | Total $E_o$/(°) |
|---|---|---|---|---|
| 20 | 10 | 0.625 | $0.42 \pm 0.54$ | $0.64 \pm 0.74$ |
| 25 | 10 | 0.618 | $0.41 \pm 0.51$ | $0.63 \pm 0.75$ |
| 30 | 10 | 0.612 | $0.44 \pm 0.51$ | $0.64 \pm 0.72$ |

the system include, in addition to the three factors in Table 6, the efficiency of the computer in solving the data. Several experiments have verified that the rate of solving the position and attitude of the PM and displaying the results in 3D plot via a computer interface can up to 16.1 Hz (966 times in 1 min, $966/60 = 16.1$ Hz).

### 3.5 Comparison with Existing Work

In order to comprehensively evaluate the performance of the tracking system, it is compared with some methods reported in the literature. The comparison of the 8 methods in terms of the PM size, tracking range, localization error, orientation error, and the execution time is shown in Table 7. It can be seen from Table 7 that our system has strong advantages in tracking accuracy. The hardware platform and optimized LM algorithm play important roles. Because the system's accurate tracking is based on the sensor (MAG3110), which can collect data with effective change when the PM moves a very small distance. Then the optimization LM algorithm provides the exact solution. Finally, the tracking system with an execution time of 0.062 s can meet the real-time requirement in most application scenarios.

**Table 6 Transmission rate of hardware**

| Hardware | Rate/Hz |
|---|---|
| Sensor (sampling) | 80 |
| Multiplexer module (transmission) | $1 \times 10^6$ |
| IIC bus (transmission) | $2 \times 10^8$ |

**Table 7 Comparison of tracking accuracy between different methods**

| Method | PM size/ (mm × mm) | Tracking range/ (mm × mm × mm) | Localization error/mm | Orientation error/(°) | Execution time/s |
|---|---|---|---|---|---|
| LM[8] | 10 × 15 | 180 × 180 × 105 | 5.2 | 6.6 | — |
| Linear-LM[11] | 5 × 6 | 500 × 500 × 500 | 1.8 | 1.6 | 0.1 |
| PSO-LM[12] | 11 × 18 | 500 × 400 × 300 | 0.003 | 0.036 | 830 |
| Graph optimization[14] | 10 × 10 | 165 × 165× (66—86) | 0.78 | 1.39 | 0.026 |
| HFFNN-LM[15] | 10 × 10 | 180 × 180 × 40 | 0.7 | 0.9 | 0.001 |
| Deep neural network[16] | 4.8 × 1.6 | 40 × 60 × 70 | 1.4 | — | — |
| PKBPNN[17] | 10 × 10 | 150 × 150 × 400 | 3.48 | 4.31 | — |
| Proposed method | 10 × 10 | 250 × 250 × 150 | 0.58 | 0.72 | 0.062 |

Note: "—" indicates that the content of this part is not clear in the literature.

## 4 Conclusion

A high-precision real-time tracking system based on the magnetic moment measurement approach and the optimized LM algorithm was proposed. First, the hardware platform of the tracking system is built. Then, the magnetic moment of the PM is calculated by using the sensing data. Next, the PC (using MATLAB) solves the position and orientation of the PM based on the optimized LM algorithm. Next, the tracking results are displayed in 3D plot via a computer interface in real time. Finally, the tracking performance is evaluated by moving the PM in the possible positions and attitude, e.g, some points fixed by the robotic arm or some specific spatial lines. From the experiments, we observe that satisfactory performance is obtained with the average localization error 0.58 mm and average orientation error 0.72° when the PM's movement is within the tracking range. Compared with other systems, obviously, our system has better performance. We will investigate the magnetic actuation methods to integrate into our proposed system in the future work.

**Conflict of Interest** The authors declare that they have no conflict of interest.

## References

[1] KIM S, BAE S, LEE W, et al. Magnetic navigation system composed of dual permanent magnets for accurate

position and posture control of a capsule endoscope [J]. *IEEE Transactions on Industrial Electronics*, 2024, **71**(1): 739-748.

[2] YUAN C Q, WANG Y, LIU J. Research on multi-sensor fusion-based AGV positioning and navigation technology in storage environment [J]. *Journal of Physics*: *Conference Series*, 2022, **2378**(1): 012052.

[3] CHEN Z R, ZHAO Y X, LIU X K, et al. Embedded position detecting method for permanent magnet linear motor systems [J]. *IEEE Transactions on Instrumentation and Measurement*, 2021, **70**: 9514010.

[4] WANG R H, PAN X W, WANG Q H, et al. Rotor position recognition technology of permanent magnet linear synchronous motor based on sliding mode observer [J]. *Journal of Physics*: *Conference Series*, 2021, **2125**(1): 012029.

[5] SCHLAGETER V, BESSE P A, POPOVIC R S, et al. Tracking system with five degrees of freedom using a 2D-array of Hall sensors and a permanent magnet [J]. *Sensors and Actuators A*: *Physical*, 2001, **92**(1/2/3): 37-42.

[6] HU C, MENG M Q, MANDAL M. Efficient magnetic localization and orientation technique for capsule endoscopy [C]//*2005 IEEE/RSJ International Conference on Intelligent Robots and Systems*. Edmonton: IEEE, 2005: 628-633.

[7] PHAM D M, AZIZ S M. A real-time localization system for an endoscopic capsule using magnetic sensors [J]. *Sensors*, 2014, **14**(11): 20910-20929.

[8] SONG S, WANG S, YUAN S S, et al. Magnetic tracking of wireless capsule endoscope in mobile setup based on differential signals [J]. *IEEE Transactions on Instrumentation and Measurement*, 2021, **70**: 4005208.

[9] SU S J, ZENG X P, SONG S, et al. Positioning accuracy improvement of automated guided vehicles based on a novel magnetic tracking approach [J]. *IEEE Intelligent Transportation Systems Magazine*, 2020, **12**(4): 138-148.

[10] HU C, MENG M Q H, MANDAL M. A linear algorithm for tracing magnet position and orientation by using three-axis magnetic sensors [J]. *IEEE Transactions on Magnetics*, 2007, **43**(12): 4096-4101.

[11] HU C, LI M, SONG S, et al. A cubic 3-axis magnetic sensor array for wirelessly tracking magnet position and orientation [J]. *IEEE Sensors Journal*, 2010, **10**(5): 903-913.

[12] SONG S, LI B P, QIAO W, et al. 6-D magnetic localization and orientation method for an annular magnet based on a closed-form analytical model [J]. *IEEE Transactions on Magnetics*, 2014, **50**(9): 5000411.

[13] SU S J, YANG W N, DAI H D, et al. Investigation of the relationship between tracking accuracy and tracking distance of a novel magnetic tracking system [J]. *IEEE Sensors Journal*, 2017, **17**(15): 4928-4937.

[14] SU S J, DAI H D, CHENG S Y, et al. A robust magnetic tracking approach based on graph optimization [J]. *IEEE Transactions on Instrumentation and Measurement*, 2020, **69**(10): 7933-7940.

[15] QIN Y D, LV B W, DAI H D, et al. An hFFNN-LM based real-time and high precision magnet localization method [J]. *IEEE Transactions on Instrumentation and Measurement*, 2022, **71**: 2509009.

[16] SEBKHI N, SAHADAT N, HERSEK S, et al. A deep neural network-based permanent magnet localization for tongue tracking [J]. *IEEE Sensors Journal*, 2019, **19**(20): 9324-9331.

[17] LV B W, CHEN Y G, DAI H D, et al. PKBPNN-based tracking range extending approach for TMR magnetic tracking system [J]. *IEEE Access*, 2019, **7**: 63123-63132.

[18] JIANG H, ZHOU Y, YANG Y. Research on permanent magnet magnetic measurement method based on equivalent magnetic moment [J]. *Electronics World*, 2016(13): 90-91 (in Chinese).

[19] PENG Q L, SUN J, ZHAO G Y, et al. Principle and software design of helmhotz coil measurement system [J]. *High Energy Physics and Nuclear Physics*, 2001, **25**(9): 920-925 (in Chinese).

[20] ZHANG H, LI Y H, LI Z. 6-D spatial localization of wireless magnetically actuated capsule endoscopes based on the fusion of hall sensor array and IMU [J]. *IEEE Sensors Journal*, 2022, **22**(13): 13424-13433.